Characteristics of Internal Fatigue Fracture of Shot-Peened Spring Steels

Maya Sugimoto[1, a] and Kenji Kanazawa[2,b]

[1] Graduate School of Science and Engineering, Chuo University, 1-13-27 Kasuga, Bunkyo-ku, Tokyo, 112-0003, Japan

[2] Department of Precision Mechanics, Chuo University, 1-13-27 Kasuga, Bunkyo-ku, Tokyo, 112-0003, Japan

[a] sugimoto@material.mech.chuo-u.ac.jp, [b] kanazawa@mech.chuo-u.ac.jp

Keywords: internal fatigue fracture, fish-eye, shot-peening, spring steel, slack quenching structure

Abstract. In order to understand internal fatigue fracture of shot-peened spring steels, high-cycle fatigue tests were carried out, and origins and shapes of fish-eyes observed on fracture surfaces were discussed.

The fatigue limit was not recognized in *S-N* plots up to 10^8 stress cycles and the internal fracture with the fish-eye was dominant. At origins of the fish-eyes, non-metallic inclusions or microstructural defects were observed.

The peak positions of distributions of depths of the origins from the specimen's surface were deeper a little than depths of crossing points of residual stress distributions. This result indicates that the internal fatigue crack is initiated at an area where the maximum stress of cyclic stress by superposing the residual stress and the applied cyclic stress is high.

The value of r_s/r_c was paid an attention to describe the shape of the fish-eye, where r_s and r_c are distances from the origin to edges of the fish-eye in directions of surface and center respectively. The values of r_s/r_c were less than unit for fish-eyes, which depth of the origin from the surface was shallow. This result means that crack propagation toward the surface is delayed compared with toward the center and can be explained by the existence of the compressive residual stress at the surface layer.

In the case of origins of fish-eyes being microstructural defects, the shapes on fracture surfaces were polygonal facets or narrow bands. According to results of microstructural observations and hardness tests, the defects were slack quenching structures SQS such as lower bainitic structures, and were formed flatly along prior austenitic grain boundaries. The fatigue crack was initiated at an interface between SQS and the matrix of martensitic structure. The shapes of defects at the origin of the fish-eye on the fracture surface were considered to depend on the relationship between the direction of loading axis and the normal direction of the flat SQS at the origin.

Introduction

Shot-peening treatments are performed frequently to components of machines and structures to increase fatigue strength of the components. In the cases of high strength steels and surface hardened steels such as shot-peened steels, stepwise *S-N* curves were obtained where two groups of fatigue data were recognized, one below about 10^6 cycles and the other beyond about 10^7 cycles. The fracture in the first group is caused by ordinary microcrack initiation and propagation from the specimen's surface, while in the second group fatigue cracks are initiated and propagate from the inside of the specimen, where the fish-eye pattern can be observed on the fracture surface.

To clarify internal fatigue fracture, many researchers have discussed about mechanisms of formation of fish-eye, especially about the early stage of crack formation from defects such as non-metallic inclusions and about kinds and size of inclusions at the origins of the fish-eyes [1,2]. However, few studies about defects except for inclusions at the origins of the fish-eyes have been

carried out [3,4].

In order to understand internal fatigue fracture of shot-peened spring steels, high-cycle fatigue tests were carried out, and origins and shapes of fish-eyes observed on fracture surfaces were discussed.

Experimental procedures

The material used was SAE9245 spring steel and the chemical compositions in mass % were as follows: C ; 0.63, Si ; 1.46, Mn ; 0.65, P ; 0.012, S ; 0.008 and Cr ;0.72. The hourglass type specimen was used which sizes at the minimum cross section were 4mm in diameter and 20mm in radius of curvature. The heat treatments of quenching and tempering were performed for roughly machined specimens. After final machining, the specimens were shot-peened under three different conditions to obtain different hardness and residual stress distributions at the surface layer of the specimen.

The conditions of shot-peening treatments are shown in Table 1 with results of shot-peening treatments. The depth of hardened layer of the shot-peened specimen was corresponding with the depth of crossing point d_{cp}, where residual stress changes from compressive to tensile stress.

Designation of specimens		A	B	C
Shot peening conditions	Shot diameter [mm]	0.3	0.3	0.6
	Shot hardness [HV]	700	550	700
	Peening velocity [m/s]	40	40	80
	Peening time [s]	75	105	60
Results of shot peening treatments	Surface roughness [μm]	4.8	4.2	15.6
	Residual stress at surface [MPa]	-875	-700	-600
	Depth of crossing point d_{cp} [μm]	90	100	260

Table 1 Conditions and results of shot-peening treatments.

Fatigue tests were carried out up to 10^7 or 10^8 stress cycles at room temperature in air by using a cantilever type rotating bending machine or an uniaxial loading machine.

The fracture surfaces were observed by using an optical microscope and a scanning electron microscope SEM. In order to clarify qualities of microstructures and defects observed on the fracture surfaces, an electron probe microanalyzer EPMA was used.

Results and discussion

***S-N* plots.** Figure 1 shows *S-N* plots of fatigue tests under the rotating bending condition. Solid and open plots indicate fracture modes of surface fracture and internal fracture with fish-eye pattern, respectively. Internal fracture with fish-eye was dominant and surface fracture occurred for a few

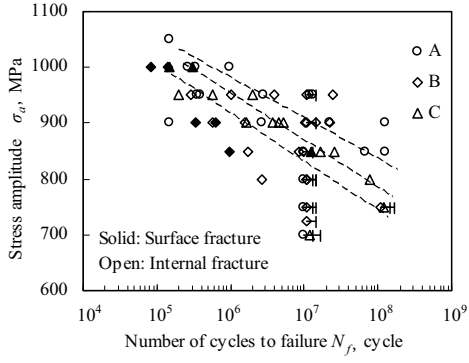

Fig.1 *S-N* plots under the rotating bending condition.

specimens shot-peened under conditions of B and C. As regions of data plots for surface fracture and for internal fracture overlapped each other, stepwise *S-N* plots were not obtained. The fatigue endurance limits could not be recognized under fatigue tests up to 10^8 stress cycles. The fatigue strengths at 10^7 cycles for A, B and C specimens were 900, 800 and 850MPa respectively.

As for results of fatigue tests under the uniaxial loading condition, the fatigue lives were small a little compared with those under the rotating bending condition and internal fracture occurred for all specimens tested.

Configurations of fish-eyes. Figure 2 shows examples of the fish-eye on fracture surface for A, B and C specimens under the rotating bending condition. The sizes of the fish-eyes of A and B specimens resemble each other, but that of C specimen is large obviously. Figure 3 is images of fish-eye under the unaxial loading condition. Sometimes very large fish-eyes were observed. A parameter *d* shown in legends of Figs.2 and 3 indicates the depth of the origin site of fish-eye from the specimen's surface. The size of the fish-eye depends on *d* basically.

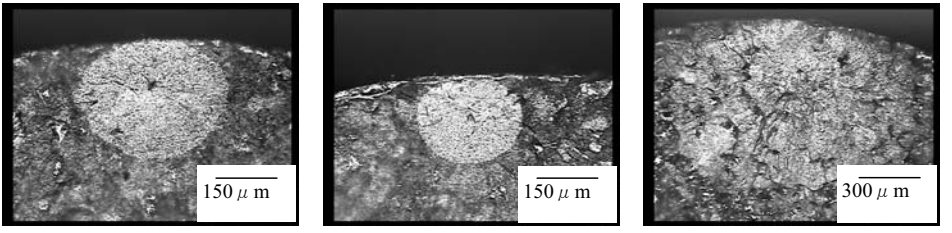

(a) A, $\sigma_a = 950$ MPa, $N_f = 1.12\times10^7$, $d = 130\ \mu$ m

(b) B, $\sigma_a = 900$ MPa, $N_f = 5.65\times10^5$, $d = 95\ \mu$ m

(c) C, $\sigma_a = 950$MPa, $N_f = 5.60\times10^5$, $d = 270\ \mu$ m

Fig.2 Examples of the fish-eye under the rotating bending condition.

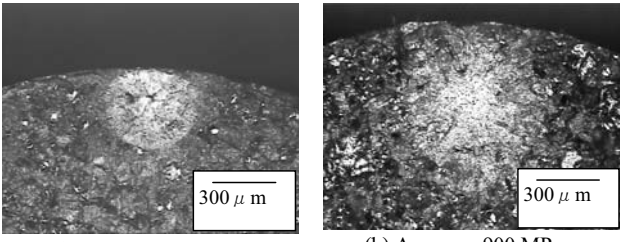

(a) A, $\sigma_a = 800$MPa, $N_f = 3.15\times10^6$, $d = 135\ \mu$ m

(b) A, $\sigma_a = 900$ MPa, $N_f = 1.39\times10^6$, $d = 380\ \mu$ m

Fig.3 Examples of the fish-eye under the uniaxial loading condition.

To discuss the depth of the origin site and the configuration of the fish-eyes, parameters for the fish-eye were defined as shown in Fig.4. Where, r_s and r_c are distances from the origin to the edges of the fish-eye in the directions of surface and center respectively. The value r_s is the same approximately as the depth of the origin site from the specimen's surface *d*.

Under the rotating bending condition, the mean values of *d* for A, B and C specimens were about

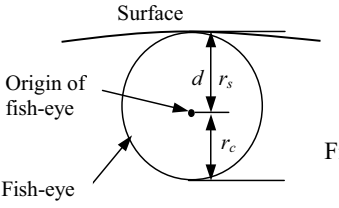

Fig.4 Parameters indicating the configuration of the fish-eye.

130, 120 and 295 μ m, respectively, which values were larger a little than the depths of crossing point d_{cp} listed in Table 1. To discuss the depth of the origin site in detail, a histogram of the depth of the origin of the fish-eye normalized by the depth of crossing point, that is, a histogram of the value of d/d_{cp} were checked. As the result, the values of d/d_{cp} ranged from 0.8 to 4.0 for the rotating bending condition, whereas the values ranged from 1.0 to 11.0 for the uniaxial loading condition. This result indicates that an internal fatigue crack is initiated at an area where the maximum stress of cyclic stress obtained by superposing the residual stress and the applied cyclic stress is high.

Next, the values of r_s/r_c were paid attention to obtain information about the process of fish-eye formation. The value of r_s/r_c had a tendency of increasing with increasing the value of d, and depended on the shot-peening conditions and the loading conditions of the fatigue tests. Figure 5 shows the relationship between d/d_{cp} and r_s/r_c. The value of r_s/r_c depends on d/d_{cp} independent of shot-peening conditions and it varys from 0.4 to 1.5 with increasing for d/d_{cp} from 0.5 to 4.0 under the rotating bending condition. Under the uniaxial loading condition the relationship between d/d_{cp} and r_s/r_c is the same as that under the rotating bending condition as long as small values of d/d_{cp}, but when the value of d/d_{cp} becomes large the value of r_s/r_c has a tendency of saturating to the unit value.

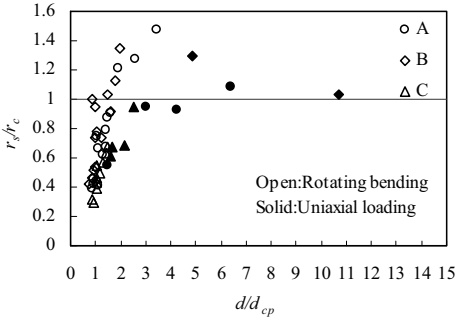

Fig.5 Relationship between d/d_{cp} and r_s/r_c.

Generally the value of r_s/r_c is larger than unit under the rotating bending condition and it becomes unit under the uniaxial loading condition, because of the difference in the stress distribution depending on the fatigue loading conditions. In the present study, there were many cases where the value of r_s/r_c was less than unit. The value of r_s/r_c being less than unit means that crack propagation toward the surface is delayed compared with toward the center. This result can be explained by the existence of the compressive residual stress at the surface layer.

When the origin site of fish-eye is located near the crossing point, that is, when the value of d/d_{cp} is nearly unit, the crack propagation toward the surface of the specimen is delayed compared with the crack propagation toward the center, because of the existence of compressive residual stress at the specimen's surface layer. As the results, the value of r_s/r_c becomes less than unit. If the origin site is located at deep position compared with the crossing point, that is d/d_{cp} being larger than unit enough, for the crack tip propagating toward the center, the normal stress amplitude applied at the tip of the crack becomes small with crack growth because of the bending stress distribution. On the other hand, for the crack tip propagating toward the specimen's surface, the normal stress amplitude applied at the tip of the crack becomes large with crack growth except for the region of surface layer where the compressive residual stress exists. Under the conditions, the crack propagation toward the surface of the specimen progresses compared with the crack propagation toward the center. As the results, the value of r_s/r_c becomes larger than unit. If the origin site is located at intermediate position of above mentioned two positions, there is a chance for the value of r_s/r_c becoming unit.

Origins of fish-eyes. Figure 6 shows examples of the origin of the fish-eye observed by using SEM. For a few cases, non-metallic inclusions were observed at the origin of the fish-eye as shown in Fig.6 (a), which inclusions were multiple ones of TiN and MnS according to EPMA observations. In

many cases, nonmetallic inclusions were not observed, but microstructural defects were observed at the origin of the fish-eye, which shapes on the fracture surfaces were polygonal facets and narrow bands as shown in Fig.6 (b) and Fig.6 (c) respectively.

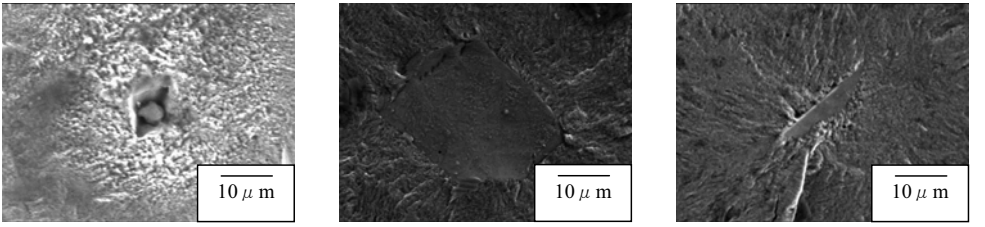

(a) A, σ_a =850MPa, N_f =1.27×10^8 (b) C, σ_a=900MPa, N_f =1.66×10^6 (c) C, σ_a=950MPa, N_f =1.30×10^7

Fig.6 Examples of the origin of the fish-eye.

To clarify the microstructural defects at the origins of the fish-eyes, matching observation and hardness tests were performed. The matching images are shown in Fig.7 where traces of indentations are due to hardness tests. The defects seem to be related to prior austenitic grain boundaries. The values of hardness of the defects for both sides were about 350HV and 530HV, and a clear difference was recognized between them.

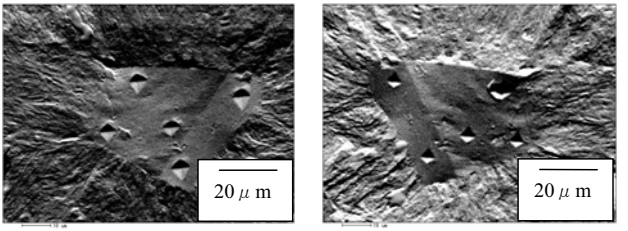

Fig.7 Matching images of microstructural defect at the origin of fish-eye.

Figure 8 (a) shows microstructures of the present material etched by using a solution of nitric acid and ethyl alcohol. As a whole the microstructures were martensitic structures, but some irregular structures where etching characteristics were differ from the martensitic structures were observed in places. The structure seems to exist along prior austenitic grain boundaries and there are two types such as a narrow band and a flat plane in the shapes. From these observations, the irregular structures are considered to be formed along prior austenitic grain boundaries with a shape of a flat plate. The difference in the shapes of the irregular structures on the photographs must be brought by how to cut the frat plate for observations.

Figure 8 (b) shows an image of the irregular structure observed with a high magnification by using SEM. As there are many streaks with the same directions each other, the structure is a lower bainite, that is, the structure is considered to be a slack quenching structure SQS. According to the hardness tests, the hardness of SQS was about 440HV, which was smaller than the hardness of 600HV for tempered martensitic structures.

Comparing this result with that obtained for the microstructural defect at the origin of the fish-eye shown in Fig.7, the microstructural defect corresponds to SQS and it is considered that a crack of the origin of the fish-eye is initiated from an interface between the SQS and the matrix of tempered martensitic structure at prior austenitic grain boundaries.

Size of defect at origin of fish-eye and feature around the defect. The size of the inclusions observed at the origin of the fish-eye is ranging from 6 to 11 μ m. Where, the size is expressed by the

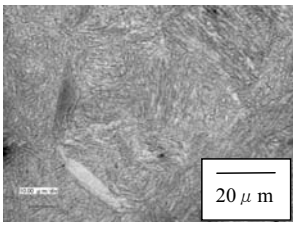

(a) Example of the microstructure by optical microscope.

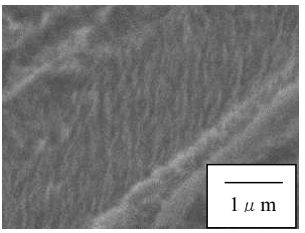

(b) Example of the SEM images of the irregular structure.

Fig.8 Microstructures of the present material.

square root of area $\sqrt{area}_{\text{DEFECT}}$, where "area" means the area of the inclusions on the fracture surface. Around the inclusions, a dark area which was named "optical dark area" ODA was observed by using an optical microscope for some specimens regardless of the size of inclusion.

The size of SQS observed at the origin of the fish-eye is widely distributed from 4 to 45 μ m, where "area" in the square root of area means the area of SQS on the fracture surface. For the SQS which size is smaller than 15 μ m at the origin of the fish-eye, ODA was observed around the SQS as shown in Fig.6 (c) as well as for some cases of inclusions.

It has been reported that the stage of formation of ODA from an inclusion is continued for the crack to grow up to a certain size, in succession, the stable crack propagation stage starts to form the fish-eye pattern, and that a large number of stress cycles are necessary to form ODA [5,6]. Figure 9 shows *S-N* plots, where the ordinate indicates the stress amplitude at the origin site of the fish-eye. Open and solid points indicate that ODA was observed around the defect at the origin of the fish-eye and that no ODA was observed, respectively. Whether the origin of the fish-eye was a non-metallic inclusion or a SQS, ODA was observed for specimens fatigued at stress cycles more than about 10^7 cycles and vice versa. The above mentioned result that a large number of stress cycles are necessary to form ODA is valid not only for the origins being inclusions but also for the origins being SQS.

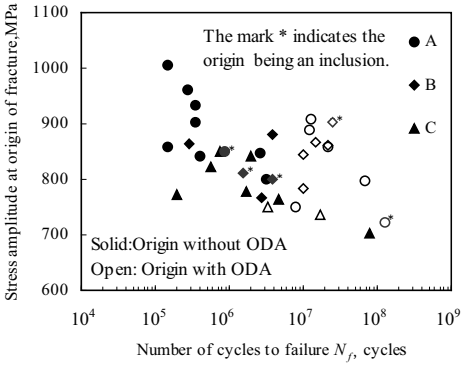

Fig.9 *S-N* plots for stress amplitude at the origin of fracture.

It has been also reported that the area of ODA increases as the number of cycles to failure N_f increases [5,6]. Figure 10 shows the relationship between N_f and $\sqrt{area}_{\text{ODA}}/\sqrt{area}_{\text{DEFECT}}$. Where, $\sqrt{area}_{\text{DEFECT}}$ is the size of defect at the origin of the fish-eye such as nonmetallic inclusion or SQS and $\sqrt{area}_{\text{ODA}}$ is the size of ODA including the size of the defect. The value of $\sqrt{area}_{\text{ODA}}/\sqrt{area}_{\text{DEFECT}}$ increases with N_f. This result indicates that the bigger the size of ODA, the larger the number of stress cycles is necessary to form it. Also from this point of view, there is no difference between circumstances for the origins of the fish-eyes being a non-metallic inclusions and SQS.

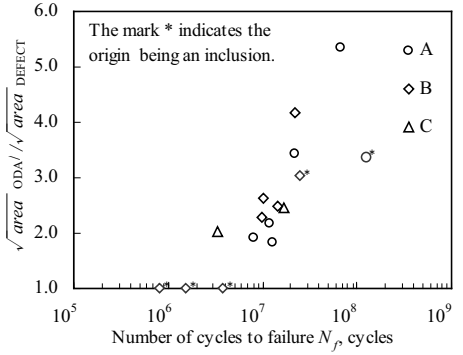

Fig.10 Relationship between $\sqrt{area}_{ODA}/\sqrt{area}_{DEFECT}$ and N_f.

Crack initiation from SQS at the origin of the fish-eye. As shown in Fig.10, in the relationship between formations of ODA and fatigue lives, the same tendency has obtained for the internal fractures originated from SQS and from non-metallic inclusions. But if SQS is regarded to be the same defect as non-metallic inclusion for sites of origins of fish-eyes, some contradiction occurs. In the case of non-metallic inclusions, it has been considered that the biggest one in the risky volume being under the severe stress conditions is the most important for fatigue crack initiation site, that is, for the origin of fish-eye[1]. But in the case of SQS, small SQS accompanying with ODA were observed on the fracture surfaces, nevertheless there had to be many big SQS in the size of area projecting SQS on the perpendicular plane to the loading direction.

Crack initiation from SQS at the origin of the fish-eye is considered as follows. The crack is not initiated at the same time at the whole interface between SQS and the matrix of martensitic structures. The crack is initiated at a part of the interface such as an edge of SQS at first. Evidence supporting this opinion is shown in Fig.11. There is a small smooth region at a part of corner of the polygonal facet and the region is considered to be a crack initiation site at the SQS.

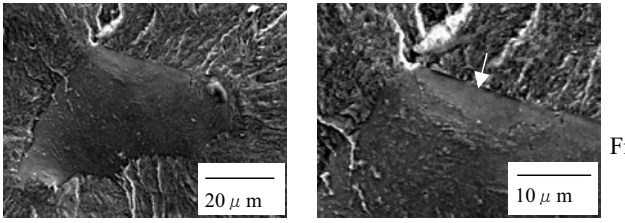

Fig.11 Example of crack initiation site at SQS of the origin of the fish-eye.

After that, there are two cases in the process of crack growth. In the first case, the crack grows along the interface of SQS with a shape of a flat plate and then a large polygonal facet of SQS was observed at the origin of the fish-eye. After this process the stable crack propagation stage can start from this SQS, where it is not necessary to form ODA and fatigue life is not so long. In the second case, the crack grows into the matrix forming ODA and then a narrow band of SQS was observed at the origin of fish-eye accompanying with ODA, where a large number of stress cycles are necessary to form ODA. Which processes of crack growth occur is considered to depend on the relationship between the direction of loading axis and the normal direction of SQS with a shape of a flat plate.

The largest size of the polygonal facet of SQS observed at the origin of the fish-eye was 45 μ m. Applying the approach of statistics of extreme values to the present material, the maximum values of the size of SQS could be estimated as 50 μ m, which value is larger a little than the maximum size of SQS observed at the origin of the fish-eye.

Conclusions

In order to understand internal fatigue fracture of shot-peened spring steels, high-cycle fatigue tests were carried out and the origins and shapes of fish-eyes on the fracture surfaces were discussed. The results obtained are summarized as follows.

(1) Stepwise *S-N* curves and fatigue limits were not recognized by fatigue tests up to 10^8 stress cycles. Internal fracture with fish-eye pattern was dominant, and at the origin of the fish-eye non-metallic inclusions or microstructural defects, which shapes were polygonal facets or narrow bands, were observed.

(2) The peak positions of distributions of depths of the origins of the fish-eyes from the surface were deeper a little than depths of crossing points of residual stress distributions, where the maximum stress of cyclic stress by superposing the residual stress and the applied cyclic stress is high.

(3) The values of r_s/r_c were less than unit for fish-eyes, which depths of the origins from the surface were shallow. This result means that crack propagation toward the surface is delayed compared with toward the center and can be explained by the existence of the compressive residual stress at the surface layer.

(4) For specimens fatigued over about 10^7 stress cycles, areas of ODA were observed around the origin of the fish-eye for both types of defects of non-metallic inclusion and SQS. The size of ODA increased with increasing fatigue lives.

(5) The microstructural defects at origins of the fish-eye were slack quenching structures SQS such as lower bainitic structures formed along prior austenitic grain boundaries. The fatigue crack was initiated at a part of the interface such as an edge of SQS. The shapes of defects at the origin of the fish-eye on the fracture surface were considered to depend on the relationship between the direction of loading axis and the normal direction of the flat SQS at the origin.

References

[1] Y. Murakami, “Material fatigue: effects of small defects and nonmetallic inclusions” (1993) Yokendo Ltd.

[2] Y. Ochi and T. Sakai, “Fundamentals and recent topics on fatigue: III Fatigue of metallic materials in the very high cycle regime”, Journal of the Society of Material Science, Japan, Vol.52, No.4, pp.433-439 (2003).

[3] T. Toriyama, Y. Murakami, T. Yamashita, K. Tsubota and K. Furumura, “Inclusion rating by statistics of extreme for electron beam remelted super clean bearing steel and its application to fatigue strength prediction”, The journal of the Iron and Steel Institute of Japan, Vol.81, No10, pp.1019-1024 (1995).

[4] Y. Kuroshima, M. Shimizu and K. Kawasaki, “Fracture mode transition in high cycle fatigue of high strength steel”, Transactions of the Japan Society of Mechanical Engineers, Vol.A-59, No.560, pp.1001-1006 (1993).

[5] K. Shiozawa, “Research trends of very high cycle fatigue in high strength steels”, Nachi Tech Rep, Vol.14 No.A1-D1 Page.A1.1-A1.11 (2007).

[6] Y. Murakami, T. Ueda, T. Nomoto and Y. Murakami, “Mechanism of superlong fatigue failure in the regime of N>10^7cycles and fractography of the fracture surface”, The journal of the Iron and Steel Institute of Japan, Vol.66, No642, pp.311-319 (2000).